Metabolic Imaging with the DCS-120 Confocal FLIM System: Simultaneous FLIM of NAD(P)H and FAD

Wolfgang Becker, Axel Bergmann, Lukas Braun

Becker & Hickl GmbH, Berlin, Germany

Abstract: We describe a metabolic imaging system based on simultaneous recording of lifetime images of NAD(P)H and FAD. The system is based on the bh DCS-120 confocal scanning FLIM system. It uses one-photon excitation by ps diode lasers, scanning by galvanometer mirrors, confocal detection, and two parallel TCSPC FLIM recording channels. The two lasers, with wavelengths of 375nm and 405 nm, are multiplexed to alternatingly excite NAD(P)H and FAD. One FLIM channel detects in the emission band of NAD(P)H, the other in the emission band of FAD. The FLIM data are processed by SPCImage data analysis software. For both channels, the data analysis delivers images of the amplitude-weighted lifetime, tm, the component lifetimes, t1 and t2, the amplitudes of the components, a1 and a2, and the amplitude ratio, a1/a2. Moreover, it delivers the fluorescence-lifetime redox ratio (FLIRR), a_{2nadh}/a_{1fad}. We demonstrate the performance of the system at the example of human bladder cells. Normal cells and tumor cells were discriminated by the tm images, the a1 images, and the FLIRR images.

Fluorescence Decay Functions of NAD(P)H and FAD

NAD(P)H (nicotinamide adenine (pyridine) dinucleotide) and FAD (flavin adenine dinucleotide) are coencymes involved in the cell metabolism. Both NAD(P)H and FAD are fluorescent. FAD and, especially, NAD(P)H are unique in the sense that their fluorescence intensities and fluorescence decay functions bear direct information on the metabolic state of the cells.

It is known that the fluorescence lifetimes of NAD(P)H and FAD depend on the binding to proteins [8, 9, 11]. Unbound NAD(P)H has a fluorescence lifetime of about 0.3 to 0.4 ns. Bound NAD(P)H has a lifetime of about 1.2 ns [9]. However, the lifetimes may vary. We have found up to 600 ps for the unbound component, and for the bound component lifetimes up to 5 ns have been reported [9]. For FAD the effect of binding is opposite: Bound FAD has a lifetime of a few 100 ps, unbound FAD of a few ns.

The ratios of the amounts of bound and unbound NAD(P)H and of bound and unbound FAD depend on the type of the metabolism. A cell can run both a reductive metabolism (glycolysis) and an oxidative one (oxidative phosphorylation). A shift from glycolysis to oxidative phosphorylation or back results in a change in the unbound/bound ratios. Thus, the bound/unbound ratios reflect the 'Warburg Effect': In normal cells oxidative phosphorylation dominates, in cancer cells reductive glycolysis [21, 22].

The a1/a2 Ratio

In intensity (or spectral) images the fluorescence components from the bound and unbound states are almost indistinguishable. In FLIM data they can easily be separated by double-exponential decay analysis. The ratio on the amplitudes of the decay components, a1/a2, often called 'amplitude ratio', directly represents the concentration ratio of unbound/bound NADH or bound/unbound FAD, see Fig. 1.

A change in the in a1/a2 ratios therefore indicates a change in the metabolism of a cell. A shift towards high a1/a2 in the NAD(P)H decay (high unbound/bound ration) indicates a shift to glycolyis and, possibly, to cancerous behaviour.

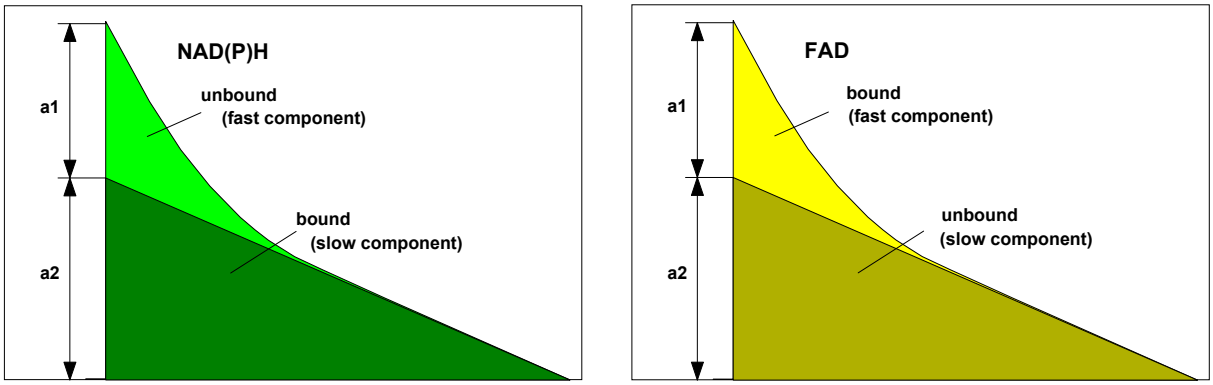

Fig. 1: Composition of the decay functions of NAD(P)H and FAD

A similar, yet less pronounced effect exists for FAD. Normally, the lifetime (or a1/a2) variation is smaller than for NAD(P)H. Therefore, a direct use of the FAD fluorescence for metabolic FLIM has not been reported yet. FAD decay parameters are, however, being used to supplement metabolic imaging by NAD(P)H.

Amplitude of the fast decay component, a1

The a1/a2 ratio directly represents the unbound/bound an bound/unbound ratio of NAD(P)H and FAD, respectively. It's use may appears attractive to describe the metabolic state. However, the a_1/a_2 has a disadvantage. Because $a_1 + a_2 = 1$ the a_1/a_2 ratio can also be expressed as

$a_1/a_2 = a_1 / (1-a_1)$

That means, the a_1/a_2 ratio is a nonlinear function of a_1. This is no problem as long as a_1 remains in the range around 0.5 to 0.6. However, if a_1 gets higher than 0.8 (which is often the case for FAD) the function becomes highly nonlinear. It is then hard to evaluate the pixel histograms. These get more and more stretched toward larger a_1/a_2 values - please note that a_1 goes to infinity for $a_1=1$. We therefore find it more useful to base the evaluation of metabolic FLIM data on the amplitude coefficient of the fast component, a1.

Amplitude-Weighted Lifetime

Often the amplitude-weighted lifetime,

$t_m = a_1t_1 + a_2t_2$

is used instead of the amplitude ratio or the amplitude of the fast component. This approach delivers data of relatively low noise but the results are only comparable as long as the component lifetimes, t_1 and t_2, remain constant. This is not necessarily the case, as has been shown by Schäfer et al. [12, 13]. In our own measurements we have found differences in the component lifetimes in the range of almost 1:2 for different cells and tissues. In other words, there is no fixed t_m value that discriminates between normal cells and tumor cells.

Redox Ratio

Both NAD(P)H and FAD form redox pairs. NAD(P)H is fluorescent in its reduced form but loses fluorescence when oxidised to NAD^+. FAD is fluorescent when oxidised to FAD^+, and loses

fluorescence when reduced. The fluorescence intensity ratio of FAD and NAD(P)H therefore changes with the redox state of the tissue. Chance et al. [6, 7] defined a 'Redox Ratio' which is

$$RR = I_{FAD} / I_{NAD(P)H} ,$$

with I_{FAD} and $I_{NAD(P)H}$ being the fluorescence intensities of FAD and NAD(P)H. Please note that also the reciprocal definition is used, i.e. $RR = I_{NAD(P)H} / I_{FAD}$.

Like the a_1/a_2 ratio or the a_1 amplitude, the redox ratio indicates whether the metabolism in a cell is more oxidative (oxidative phosphorylation) or more reductive (glycolysis). For practical applications please see [15, 16, 18, 20]. Unfortunately, measurements of the redox ratio suffer from the same problems as all intensity-based methods: The result not only depends on the redox state itself but also on the concentration ratio of NAD(P)H and FAD. Moreover, instrumental imperfections, such as changes in the laser power, focus drift, or image shift between the recording of the NAD(P)H and the FAD data have an influence on the result. Also chromatic aberration of the microscope lens can have an influence.

OMI Index

Skala and Walsh combined the normalised value of the redox ratio RR, the normalised amplitude-weighted fluorescence lifetime, $\tau_{m\ NADH,}$ and the normalised $\tau_{m\ FAD,}$ of NAD(P)H and FAD into a single 'Optical Molecular Imaging', or OMI index. High OMI means a shift toward glycolysis and cancer metabolism [19, 20].

Fluorescence-Lifetime Redox Ratio (FLIRR)

To navigate around the problems of the classic redox ratio Alam et al. [1] and Wallrabe et al. [17] defined a fluorescence-lifetime redox ratio (FLIRR). It is the ratio of the fractional amplitudes of the bound decay components of NAD(P)H, $a_2/(a_1+a_2)_{NADH}$, and FAD, $a_1/(a_1+a_2)_{FAD}$.

$$FLIRR = \frac{a_2/(a_1+a_2)_{NADH}}{a_1/(a_1+a_2)_{FAD}}$$

The advantage of the FLIRR is that it does not depend on the relative amounts of NAD(P)H and FAD in the cells, and not on the laser power, the focus accuracy or focus quality, or other instrument parameters.

Instrumental Considerations

Excitation and Detection Wavelengths

Approximate excitation and emission spectra of NAD(P)H and FAD are shown in Fig. 2. The spectra were taken from [9] and [14]. The figure shows that NAD(P)H needs an excitation wavelength shorter than 380 nm. FAD can be excited all the way from 350 nm to about 475 nm.

The emission spectra show that a clean NAD(P)H signal can be detected from about 425 to 475 nm. Above 475 nm the NAD(P)H signal is overlaid by emission from FAD. FAD emission occurs from about 480 nm to more than 600 nm. However, there is a strong overlap from the NAD(P)H emission. A clean FAD signal can therefore only be detected if an excitation wavelength above 400 nm is used, where excitation of NAD(P)H is negligible. In other words, the signals from NAD(P)H and FAD can only be separated if different excitation wavelengths *and* different detection wavelengths are used.

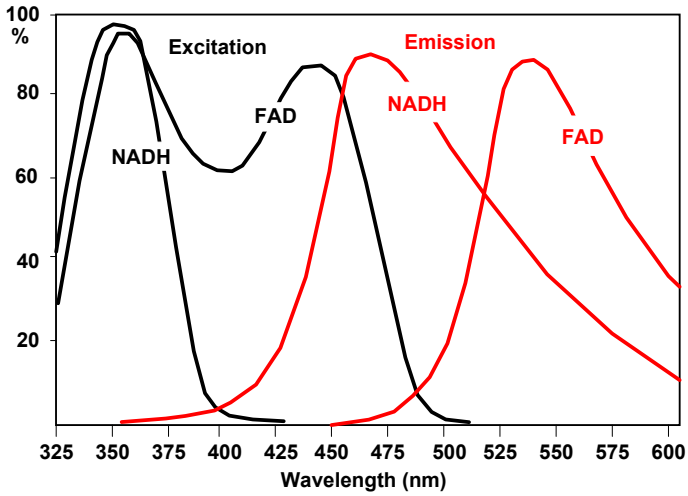

Fig. 2: Excitation and emission spectra of NADH and FAD. From bh TCSPC Handbook, after [9] and [14].

As an additional instrumental condition, the excitation wavelength for FAD should be outside the wavelength interval for NAD(P)H detection. Taking into account the availability of laser diode wavelengths there is only one possible combination:

NAD(P)H: Excitation 375 nm, Detection wavelength 420 to 470 nm

FAD: Excitation 405 nm, Detection wavelength 490 to 600 nm

TCSPC FLIM Process with Laser Multiplexing

It is desirable that the data for NAD(P)H and FAD are recorded quasi-simultaneously. This way, possible focus drift, image shift, or, importantly, changes in the metabolic state of the cells induced by the imaging process itself have the same influence on both recordings. Quasi-simultaneous measurement at two excitation wavelengths can be achieved by TCSPC FLIM in combination with laser multiplexing [2, 3, 4].

TCSPC FLIM is based on scanning the sample by a high-repetition rate pulsed laser beam and the detection of single photons of the fluorescence signal returning from the sample. Each photon is characterised by its time in the laser pulse period and the coordinates of the laser spot in the scanning area in the moment its detection. The recording process builds up a photon distribution over these parameters. The result can be interpreted as an array of pixels, each containing a full fluorescence decay curve in a large number of time channels.

To record lifetime images excited by several lasers of different wavelengths, the lasers are multiplexed in time. The multiplexing period can be anywhere from a few microsecond to about one second. To avoid aliasing with the scanning multiplexing is synchronised with the pixels, lines, or frames of the scan. The number of the laser is used as an additional coordinate of the photon distribution. The result can be interpreted as a single photon distribution that has separate decay curves for the individual lasers in their pixels, or as several photon distributions for the individual lasers [2, 3, 4]. The principle is illustrated in Fig. 3.

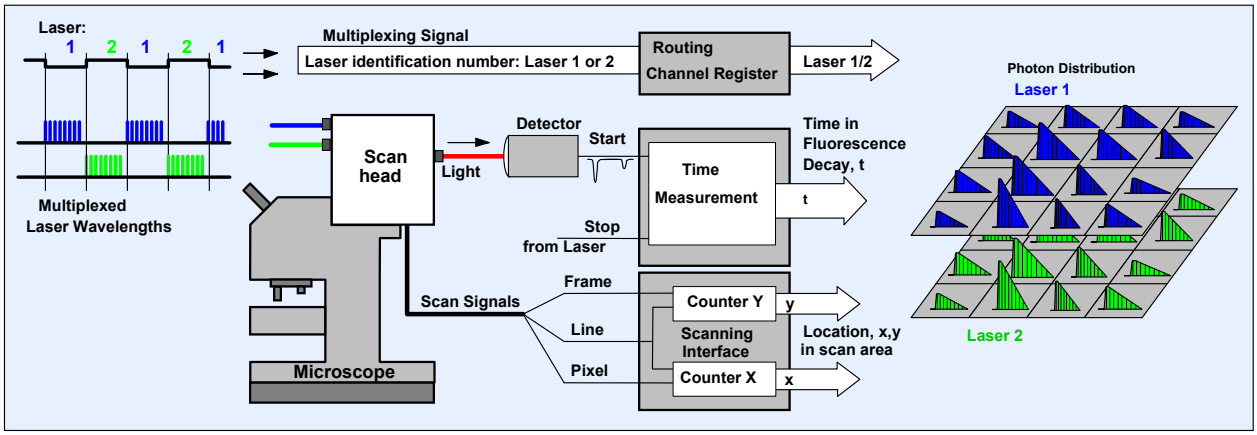

Fig. 3: Principle of TCSPC FLIM with laser wavelength multiplexing

Two such channels are operated in parallel, detecting through different filters [5]. The result are lifetime images for four combinations of excitation and detection wavelengths:

	Excitation	Emission	Signal detected
Image 1	375 nm	420 to 470 nm	NAD(P)H
Image 2	405 nm	420 to 470 nm	NAD(P)H + FAD
Image 3	375 nm	490 to 600 nm	FAD + NAD(P)H
Image 4	405 nm	490 to 600 nm	FAD

The data of interest are the ones in Image 1 (NAD(P)H) and in Image 4 (FAD).

Laser Multiplexing Control

Multiplexing of the lasers is controlled via the GVD-120 scan controller of the DCS-120 system. The lasers can be multiplexed frame by frame, line by line, or within each pixel (The last option is also used for PLIM excitation). For user interface, parameter setup, and other technical details please see Handbook of the DCS-120 system [5].

Data Analysis

Data analysis was performed by bh SPCImage software, version 7.5. The data were loaded into SPCImage directly from SPCM data acquisition software. SPCM was configured to display only the two excitation - emission combinations of interest [4]. The data were sent to SPCImage by the 'Send to SPCImage' command, with option 'All Windows'. The data showing up in SPCImage were analysed by a double-exponential decay model. False-colour tm and a1 images were created by using 'colour' 'tm' and 'colour' 'a1%', respectively. FLIRR images were created by switching to the NADH channel and using 'colour', a1% divided by a2% of the FAD channel.

Results

Representative results are shown in Fig. 5 through Fig. 7. The images were obtained from human bladder cells excised during tumor surgery. Fig. 5 shows NAD(P)H images of the amplitude-weighted lifetime, tm. The left image shows normal cells, the right image tumor cells. (The right image contains also some normal cells, especially in the upper part. This is unavoidable due to the procedure by which the cells were excised.) As expected, tm is shorter in the tumor sample.

NAD(P)H images of the amplitude, a1, of the fast decay component are shown in Fig. 5. There is a clear difference in a1 between the normal cells and the tumor cells. The normal cells have an average a1 of about 0.65 (or 65% of the total amplitude). The cancer cells have between 75% and 80%. The values are in agreement with [10]. We find similar values consistently in data of different cells.

FAD data are shown in Fig. 6. In general, also the FAD data show the expected trend. a_1 decreases for the cancer cells, indicating that they contain less bound FAD (note a_1 is the *bound* component of FAD). However, the details are not entirely plausible. On the one hand, cells in the upper part of Fig. 6, right, have a significantly different a_1 then the cells in the normal-cell sample (Fig. 6, left). On the other hand, in the NAD(P)H images the same cells have *the same* a_1 as the cells in the 'normal' sample (compare Fig. 5, left and right). However, there is a possible explanation. The redox ratio in the tumor sample may be so low that the FAD intensity gets extremely weak. It is then possible that residual NAD(P)H fluorescence excited by the 405-nm laser is detected in the FAD channel. The fluorescence in the yellow cells in Fig. 6 may then be from NAD(P)H, not FAD. A inspection of the decay curves in the yellow areas shows indeed that the decay functions are more compatible with NAD(P)H then with FAD. An improvement can probably be obtained by using a slightly longer excitation wavelength for FAD excitation.

Fig. 7 shows the FLIRR calculated from the same data sets. As expected, the FLIRR shifts to lower values for the cancer cells.

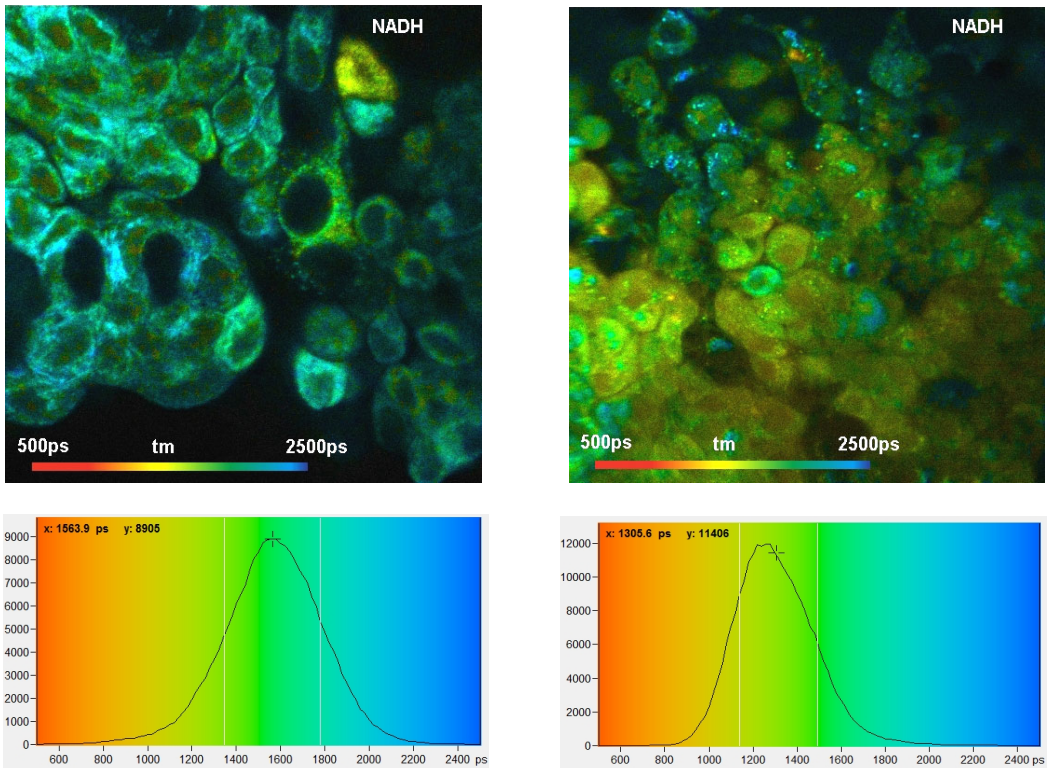

Fig. 4: NAD(P)H tm images for normal cells (left) and tumor cells (right). Lower row: Histograms of tm over the pixels of the images. As expected, tm is shorter in the tumor sample.

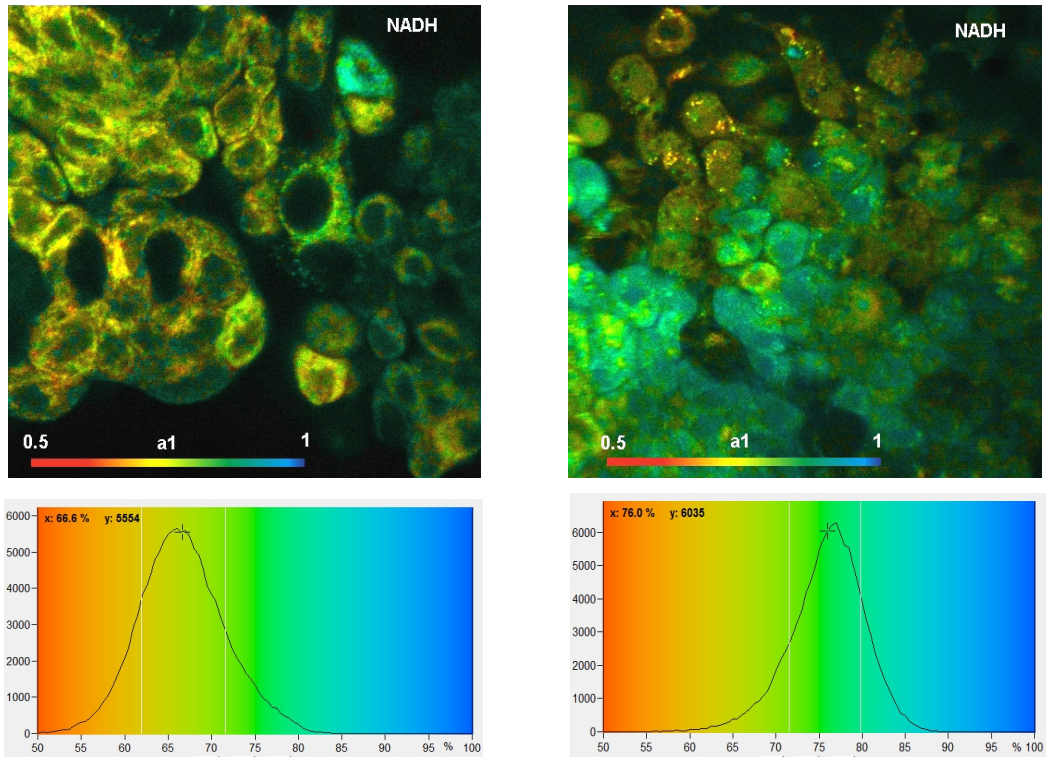

Fig. 5: NAD(P)H a1 images for normal cells (left) and tumor cells (right). Lower row: Histograms of a1 over the pixels of the images. The histogram of the tumor sample is from lower half of the image because the upper half contains also normal cells.

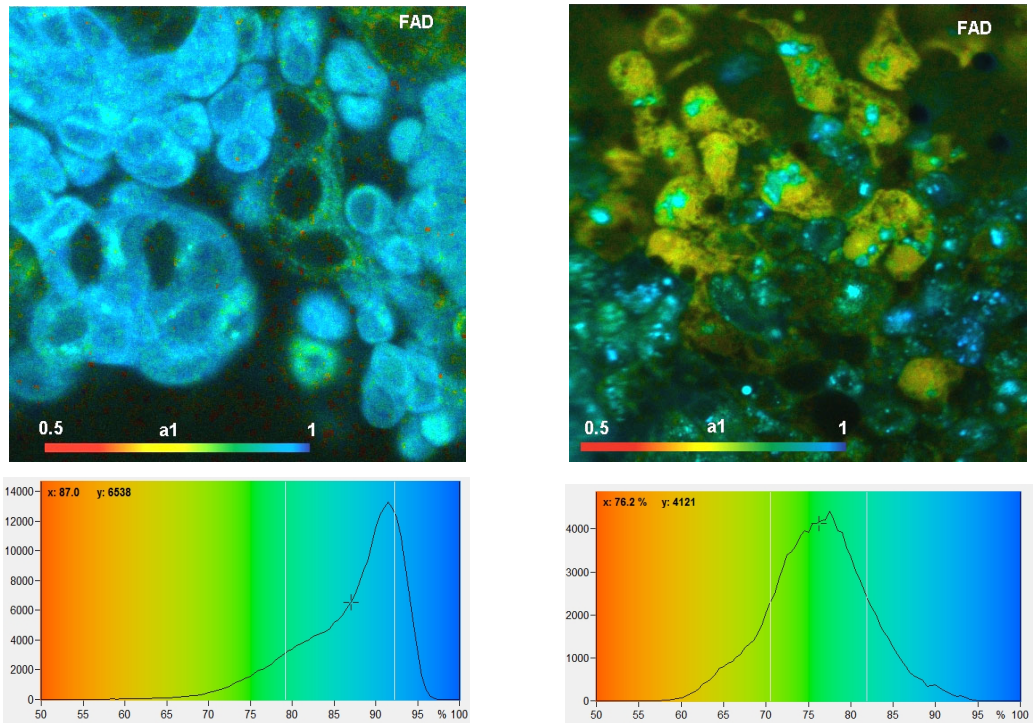

Fig. 6: FAD a1 images for normal cells (left) and tumor cells (right). Lower row: Histograms of a1 over the pixels of the images. The histogram of the tumor sample is from lower half of the image because the upper half contains also normal cells.

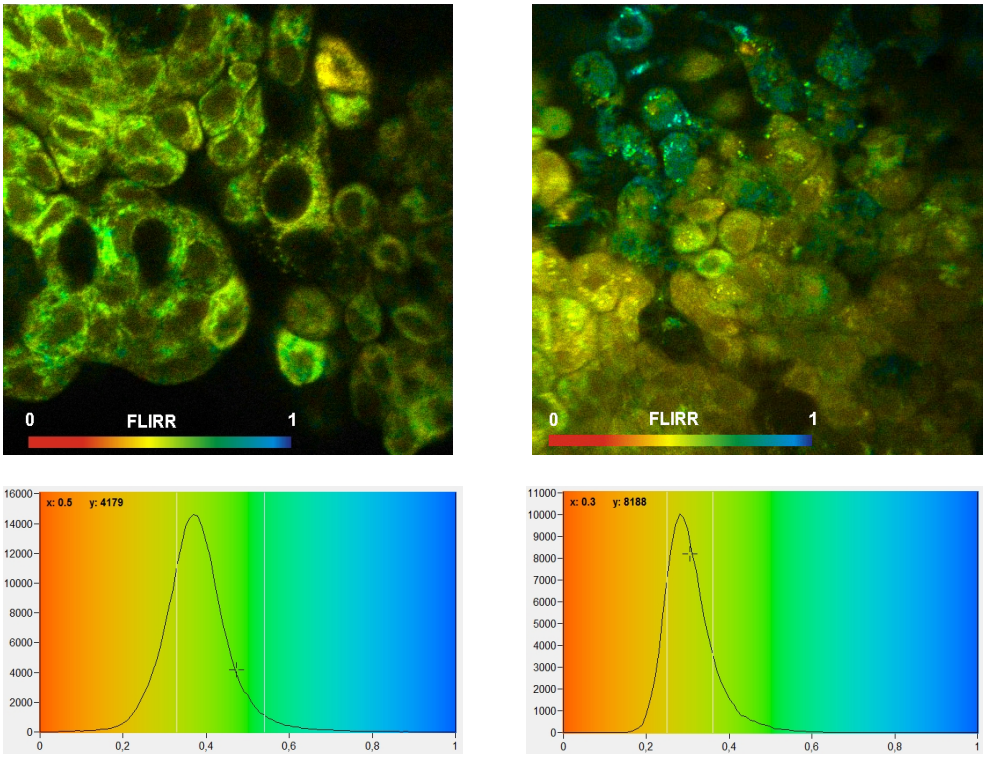

Fig. 7: FLIRR images of normal cells (left) and tumor cells (right). Lower row: Histograms of the FLIRR over the pixels of the images. The histogram of the tumor sample is from lower half of the image.

Summary

Metabolic information from live cells can be obtained from FLIM data of NAD(P)H and FAD. Both compounds appear in a bound and an unbound form. Both forms have different fluorescence lifetimes. A shift from oxydative phosphorylation to glycolysis or vice versa causes a change in the composition of the decay functions. For obvious reasons, it is desirable to record the images for NAD(P)H quasi-simultaneously. This was achieved by multiplexing two ps diode lasers, of 375nm and 405nm wavelength, and recording FLIM data into different routing channels of two TCSPC modules. One of the two modules detected in the emission range of NAD(P)H, the other in the emission range of FAD. The required recording and data analysis functions are available in the bh DCS-120 confocal Scanning FLIM System. Data recorded with this system show that the distribution of the mean lifetimes, tm, and, especially, the distribution of the amplitude of the fast decay component, a1, in the NAD(P)H and in the FAD images are different for normal cells and tumor cells. Differences were also found in the Fluorescence-Lifetime Redox Ratio, FLIRR.

Acknowledgement

The work described in this note was performed under the support of German BMBF, project ‘Endoskopische Panoramabildgebung und faseroptische Spektroskopie in der Urologie zur Multi-Dimensionalen Diagnostik’.

References

1. S. R. Alam, H. Wallrabe, Z. Svindrych, A. K. Chaudhary, K. G. Christopher, D. Chandra, A. Periasamy, Investigation of Mitochondrial Metabolic Response to Doxorubicin in Prostate Cancer Cells: An NADH, FAD and Tryptophan FLIM Assay. Scientific Reports 7 (2017)
2. W. Becker, Advanced time-correlated single-photon counting techniques. Springer, Berlin, Heidelberg, New York, 2005
3. W. Becker, Introduction to Multi-Dimensional TCSPC. In W. Becker (ed.) Advanced time-correlated single photon counting applications. Springer, Berlin, Heidelberg, New York (2015)
4. W. Becker, The bh TCSPC Handbook. 7th edition (2017). Available on www.becker-hickl.com. Please contact bh for printed copies.
5. Becker & Hickl GmbH, DCS-120 Confocal and Multiphoton FLIM Systems, user handbook, 7th edition (2017). www.becker-hickl.com. Please contact bh for printed copies.
6. B. Chance, Pyridine nucleotide as an indicator of the oxygen requirements for energy-linked functions of mitochondria. Circ Res 38, I31–I38 (1976)
7. B. Chance, B. Schoener, R. Oshino, F. Itshak, Y. Nakase, Oxidation–reduction ratio studies of mitochondria in freeze-trapped samples. NADH and flavoprotein fluorescence signals J. Biol. Chem. 254, 4764–4771 (1979)
8. J.R. Lakowicz, H. Szmacinski, K. Nowaczyk, M.L. Johnson, Fluorescence lifetime imaging of free and protein-bound NADH, PNAS **89**, 1271-1275 (1992)
9. J.R. Lakowicz, Principles of Fluorescence Spectroscopy, 3rd edn., Spriner (2006)
10. M.N. Pastore, H. Studier, C.S. Bonder, M.S. Roberts, Non-invasive metabolic imaging of melanoma progression. Exp. Dermatol. 26, 607–614 (2017)
11. R.J. Paul, H. Schneckenburger, Oxygen concentration and the oxidation-reduction state of yeast: Determination of free/bound NADH and flavins by time-resolved spectroscopy, Naturwissenschaften **83**, 32-35 (1996)
12. P.M. Schaefer, D. Hilpert, M. Niederschweiberer, L. Neuhauser, S. Kalinina, E. Calzia, A. Rueck, B. von Einem, C.A.F. von Arnim, Mitochondrial matrix pH as a decisive factor in neurometabolic imaging. Neurophotonics 4(4):045004 (2017)
13. P. M. Schaefer, S. Kalinina, A. Rueck, C.A.F. von Arnim, B. von Einem, NADH Autofluorescence - A Marker on its Way to Boost Bioenergetic Research. Cytometry Part A, 1-13 (2018)
14. D. Schweitzer, S. Schenke, M. Hammer, F. Schweitzer, S. Jentsch, E. Birckner, W. Becker, Towards Metabolic Mapping of the Human Retina. Micr. Res. Tech. 70, 403-409 (2007)
15. M.C. Skala, A. Fontanella, L. Lan, J.A. Izatt, M.W. Dewhirst, Longitudinal optical imaging of tumor metabolism and hemodynamics. J. Biomed. Opt. 15(1) 011112-1 to -8 (2010)
16. M.C. Skala, N. Ramanujam, Multiphoton Redox Ratio Imaging for Metabolic Monitoring in vivo. Methods Mol. Biol. 594, 155-162 (2010)
17. H. Wallrabe, Z. Svindrych, S. R. Alam, K. H. Siller, T. Wang, D. Kashatus, S. Hu, A. Periasamy, Segmented cell analyses to measure redox states of autofluorescent NAD(P)H, FAD & Trp in cancer cells by FLIM. Sci. Reports 8:79, 1-11 (2018)
18. A. Walsh, R.C. Cook, B. Rexer, C.L. Arteaga, M.C. Skala, Optical Imaging of metabolism in HER2 overexpressing breast cancer cells. Biomedical Optics Express 3(1), 75-85 (2012)
19. A. J. Walsh, R. S. Cook, M. E. Sanders, L. Aurisicchio, G. Ciliberto, C. L. Arteaga, M. C. Skala, Quantitative Optical Imaging of Primary Tumor Organoid Metabolism Predicts Drug Response in Breast Cancer. Cancer Res 74, OF1-OF11 (2014)
20. A. J. Walsh, M. C. Skala, Optical metabolic imaging quantifies heterogeneous cell populations. Biomed. Opt. Expr. 6, 559-573 (2015)
21. O. Warburg, On the origin of cancer cells. Science 123, 309-314 (1956)
22. O. Warburg, On respiratory impairment in cancer cells. Science 124, 269-270 (1956)

Contact:

Wolfgang Becker
Becker & Hickl GmbH
Berlin, Germany
Email: becker@becker-hickl.com
info@becker-hickl.com